Phase-sensitive LBIC analysis

Th. Pernau, P. Fath, E.Bucher
Universitaet Konstanz, Fachbereich Physik, Fach X916, D-78457 Konstanz, Germany
Tel.: +49-7531-88-3644, Fax: +49-7531-88-3895

ABSTRACT

We built a setup for local current and voltage analysis as well as reflection measurements. The sample is illuminated by four amplitude-modulated diode lasers with wavelengths of 635 nm, 835 nm, 910 nm and 980 nm coupled into one optical fibre. The phase shift introduced by the solar cell depends on carrier lifetime, carrier diffusion velocity, time delay in both instrument and sample and the impedances incorporated in the solar cell itself. At a reference frequency of 1 kHz, the phase shift introduced by carrier lifetime and diffusion dynamics is around 1°, the solar cell's internal capacitors and resistors introduce a phase shift of up to 70°. Significant structure in phase maps is only visible in the long wavelength range (833 nm, 910 nm and 980 nm).

1. INTRODUCTION

The **l**ight **b**eam **i**nduced **c**urrent (LBIC) technique is a spatially resolving characterisation method for any photosensitive device. The sample, i.e. a solar cell, is illuminated by a small light spot and the generated photocurrent or photovoltage is measured. By moving either the light spot or the sample, it is possible to record a topography. If the signal is detected by lock-in amplifiers, it is also worth looking at the phase shift introduced by the experiment. Inspired by the theory of modulated free carrier absorption (MFCA) [1], we focused on the conditions given by a solar cell.

2. EXPERIMENTAL SETUP

Details of our experimental setup can be found in [2], further LBIC systems are described in [3, 4, 5, 6, 7, 8, 9].

2.1 Principle of operation

The core of our LBIC system is an 8-channel dual-phase lock-in amplifier, whose four reference oscillators are used for the amplitude modulation of four laser diodes with the wavelengths 635 nm, 835 nm, 910 nm and 980 nm. The amplitude modulation of the lasers at different frequencies enables easy separation of the signal components as well as reflection signal R(λ) captured by the reflection measurement cells. $I_{sc}(\lambda)$ is measured using a current-to-voltage converter whereas for photovoltage measurements, the sample is directly connected to the voltage input of the lock-in amplifiers. The dual-phase lock-in amplifiers not only give signal magnitude readout, they also provide information about signal time shift, which is expressed in terms of a phase shift φ.

2.2 Signal processing with the lock-in amplifier

The lock-in amplifier is a phase and frequency sensitive AC signal analyser which enables individual signal extraction out of a sum of AC signals, even if large DC offsets or noise are present. The operating principle is discussed in detail in [2]. The lock-in amplifier is used to analyse an experiment's signal s(t), which is a function of the reference f(t).

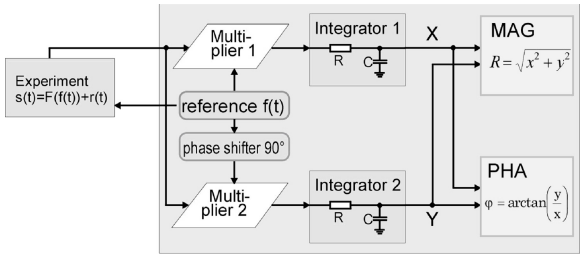

Fig. 1: The two-phase lock-in amplifier allows the extraction of an AC signal similar to the reference f(t) out of an arbitrary signal s(t). The instrument not only delivers the magnitude, but also the phase shift with respect to the reference.

3. INFLUENCE OF SOLAR CELL PARAMETERS ON PHASE SHIFT

3.1 Bulk lifetime / diffusion length

Consider a solar cell submitted to monochromatic, sine-modulated light beam:

$$(1) \quad g(x,t) = \alpha(1-R)I_0 e^{-\alpha x} e^{i\omega_0 t} + G_0(x)$$

where α is the light penetration depth, R the reflection coefficient and I_0 the incident modulated photon flux. $G_0(x)$ is a homogenous generation due to biaslight and is not detected by the lock-in amplifier, so we ignore this item. The generation invokes an excess carrier density $\Delta n(x,t)$ in the p-region. Recombination in the bulk is governed by bulk lifetime τ:

$$(2) \quad r(x,t) = \frac{\Delta n(x,t)}{\tau}$$

The generated excess carriers follow the partial differential equation:

$$(3)\quad \frac{\partial}{\partial t}\Delta n(x,t) = D_n \frac{\partial^2}{\partial x^2}\Delta n(x,t) + g(x,t) - r(x,t)$$

D_n is the diffusion constant for electrons in the p region.

As the carrier density $\Delta n(x,t)$ will have the same periodicity ω_0 as the generation $\Delta n(x,t)$, it can be expanded into a Fourier series

$$(4)\quad \Delta n(x,t) = \sum_{m=-\infty}^{\infty} \Delta n_m(x)\cdot e^{im\omega_0 t}$$

(4) substituted into (3) delivers an infinite, but countable set of differential equations with boundary conditions $\Delta n_m(0) = 0$ and $D_n \frac{\partial}{\partial x}\Delta n_m(W) = -S\Delta n_m(W)$ (W= cell thickness). All but one (m=1) of these are homogenous resulting in $\Delta n_m(x)\equiv 0$. Introducing the complex bulk lifetime $\tau^* = \frac{\tau}{1+i\omega\tau}$, the remaining inhomogeneous equation can be rewritten in the familiar form (m=1 omitted):

$$(6)\quad D_n \frac{\partial^2}{\partial x^2}\Delta n(x) = \frac{\Delta n(x)}{\tau^*} - G(x)$$

where G(x) is the single Fourier coefficient of the generation.

We are more interested in the short circuit current than in the carrier concentration, which we will express in the normalised form, the internal quantum efficiency IQE:

$$(7)\quad IQE = \frac{1}{I_0(1-R)} D_n \frac{\partial}{\partial x}\Delta n(0)$$

with the solution:

$$(8)\quad IQE = \frac{L^*\cdot\left(L^* - k\frac{1}{\alpha}\right)}{L^{*2} - \frac{1}{\alpha^2}} + \frac{e^{-\alpha W} L^*\left(\left(\frac{k}{\alpha} - L^*\right)\cosh\left(\frac{W}{L^*}\right) + \left(kL^* - \frac{1}{\alpha}\right)\sinh\left(\frac{W}{L^*}\right)\right)}{L^{*2} - \frac{1}{\alpha^2}}$$

W is the solar cell thickness, α the Absorption coefficient and S the backside recombination velocity.

$$(9)\quad k = \frac{\frac{L\cdot S}{D_n} + \tanh\left(\frac{W}{L^*}\right)}{1 + \frac{L\cdot S}{D_n}\cdot\tanh\left(\frac{W}{L^*}\right)}$$

The complex diffusion length L^* is determined by

$$(10)\quad L^* = \sqrt{D_n\cdot\tau^*}$$

The phase shift φ in the lock-in measurement is introduced by the complex IQE as follows:

$$(11)\quad \tan\varphi = \frac{\mathrm{Im}(IQE)}{\mathrm{Re}(IQE)}$$

In our experiment, the reference frequency is around 1 kHz, and assuming S=1000 cm/s, the phase shift is typically around -1°, see Fig. 2. Note that the phase shift is negative, which corresponds to a retardation of the signal.

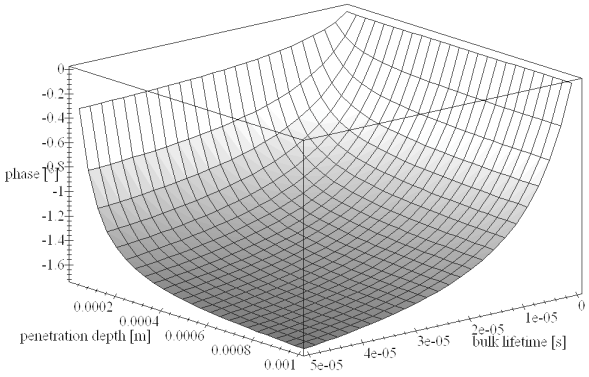

Fig. 2: LBIC phase shift introduced by carrier lifetime. Reference frequency is 1 kHz, back SRV=100 cm/s. The phase shift introduced by lifetime is negative, which corresponds to a retardation of the signal.

3.2 Phase shift introduced by capacitors and resistors

Every solar cell with space charge region incorporates a capacitance formed by the separated charges by this region. The capacitance may be approximated as if the space charge region was a plate capacitor with plate distance = width of the space charge region. Furthermore, non-ideal solar cells incorporate a parallel resistance R_p and a series resistance R_s. Additional series resistance may be introduced by the measurement apparatus itself. The solar cell's capacitance does not influence DC, steady-state operation, but is very well visible in transient and AC measurements. The capacitance C incorporated in a solar cell with space charge region width of 300 nm is

usually around 35 nF per 1 cm². For our calculation, we assumed C=35 nF/cm².

For the impedance calculation, consider a solar cell measurement setup represented by the diagram in Fig. 3.

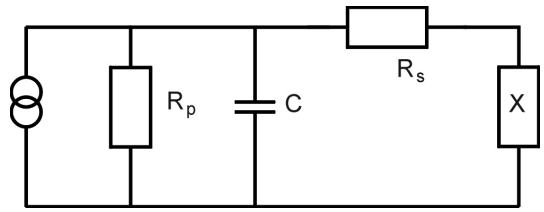

Fig. 3: simplified block diagram of a solar cell. The solar cells internal capacitor (formed by the space charge region) lies parallel to the current source and the shunt resistance. Any X<∞ represents a load connected to the solar cell which is connected in series with the series resistance. Ideal short circuit conditions are realised by X=0.

The impedance Z of the diagram in Fig. 3 introduces the phase shift

$$(12)\quad \tan\varphi = \frac{\mathrm{Im}\,Z}{\mathrm{Re}\,Z}$$

When operating the solar cell under I_{sc} conditions and $R_s << R_p$, the capacitance C is connected parallel to the shunt resistor R_s+R_M (X = R_M = internal resistor of the measurement device), this reduces the phase to

$$(13)\quad \varphi=\arctan(\omega C(R_s+R_M))$$

In good solar cells, this is unfortunately close to zero, but the series resistance can have a strong influence when investigating bad cells.

The impedance of the diagram in Fig. 3 for V_{oc} conditions (X= ∞) is:

$$(14)\quad Z = R_s + \frac{1}{\frac{1}{R_p} - i\omega C}$$

When operating with a reference frequency of 1 kHz, the magnitude of the impedance $|Z_c| = \frac{1}{\omega C}$ is in the range of the parallel resistor of an industrial type solar cell (R_p=1000-5000 Ωcm²) and introduces a considerable phase shift of up to 70°. In this case, the series resistance has nearly no influence.

4 THE EXPERIMENT

As an example, we summarise measurements of a multicrystalline industrial solar cell sized 10*10 cm². This solar cell was passed through IV analysis:

FF [%]	I_{sc} [mA/ cm ²]	V_{oc} [mV]	R_p [Ωcm²]	R_s [Ωcm²]
72.8	29.7	600	2022	1.77

Substituting the values for R_p and R_s into (14) and assuming C=35nF/cm², the phase shift between V_{oc} and I_{sc} measurement should be 26° at ω=1.1 kHz. We measured a phase shift of 21.3°. Both phase maps of I_{sc} and V_{oc} show a marginal phase shift of up to –4°, see Fig. 4.

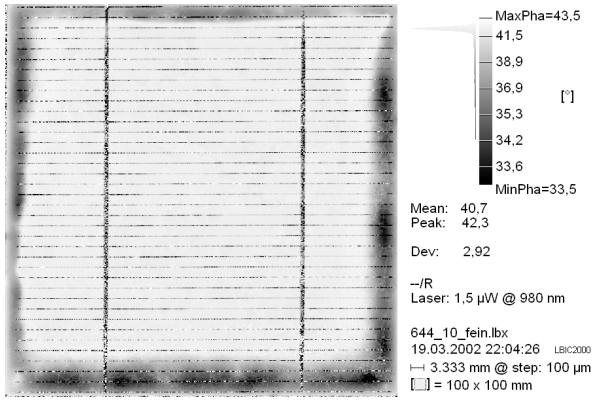

Fig. 4: Phase shift map of a 10*10 cm² mc solar cell operating under I_{sc} conditions. The scaling is not linear, this improves detail recognition.

The back side of the solar cell shown in Fig. 4 is marginally covered with LPCVD silicon nitride. The sheet thickness is 70 nm maximum at the cell edges, diminuishing to zero on a length of up to 2 cm. Due to backside silicon nitride coverage, no Al BSF was formed, see Fig. 5.

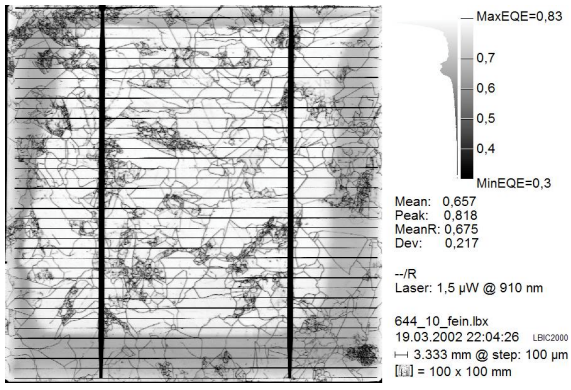

Fig. 5: EQE map of the same solar cell as shown above. The marginal grey areas are not covered by Al BSF.

Comparing the maps shown in Fig. 4 and Fig. 5, it is remarkable that the BSF uncovered region (see EQE map) and the phase shifted marginal area are not coincident. A possible explanation might be that there is a considerable contact failure in the phase shifted area, depending on rear side SiN thickness. If so, the carriers would have to spend additional time on their trip around the defect contact region, which results in a negative phase shift.

To prove this, we removed the Al contact at the upper left cell edge in Fig. 5. The result (photo) is shown in Fig. 6:

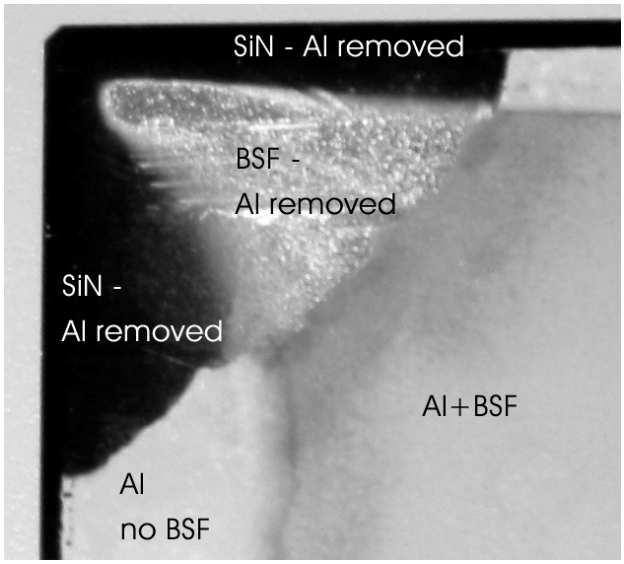

Fig. 6: Once the Al back contact is removed, it is clearly visible that the SiN below the Al is still present. This can create a severe contact failure.

The removal of the Al contact did not influence the EQE of the cell. As the LBIC system operates with a total optical power of 6 µW, the generated current is only 4 µA maximum, which is not sensitive to a prolonged current path to reach the good contact area. The phase map of the removed Al contact shows an additional phase shift of – 2° in the areas with no BSF, whereas the BSF covered areas remain unchanged. As a result, the phase map can at least detect a contact failure in the non-BSF covered region, which is not visible in the EQE map.

5 CONCLUSION

LBIC is an excellent tool to investigate spatially distributed signal generation of a solar cell. Every LBIC system using lock-in amplifiers can detect the phase shift of the signal. By recording the phase shift of both V_{oc} and I_{sc} measurements one can get additional information about local impedances and hints on abnormal contact properties. In the experiment, the analysis of the phase shift revealed a contact failure which was not visible in the phase-independent EQE map.

ACKNOWLEDGEMENTS

We would like to thank B. Fischer for the fruitful discussions on the topic and M. Keil for the technical assistance. This work was supported by the E.C. within the Fast-IQ project under contract No. ERK6-CT1999_00002.

REFERENCES

[1] F. Sanii et al., Proc. 20th IEEE Photov. Spec. Conf. 1988, p. 575-580

[2] T. Pernau et al., Proceedings of the 17th EPSEC, München 2001, VD 1.4 (to be published)

[3] M. Acciarri et al., Mater. Sci. Eng., B42 (1996) 208.

[4] G. Agostinelli et al., Proceedings of the 2nd WCPEC, Vienna, Austria, 1998, p. 184.

[5] G. Agostinelli, G. Friesen, F. Merli, E. Dunlop, M. Acciarri, A. Racz, J. Hylton, R. Einhaus, T. Lauinger, '*Large Area Fast LBIC as a Tool for Inline PV Modula and String Characterisation',* 17th EPSEC, München 2001, OA 1.2 (to be published)

[6] M. Stemmer, Appl. Surf Sci. **63** (1993), 213-217

[7] J. Carstensen, G. Popkirov, J. Bahr, H. Föll, Proc.16th EPSEC, Vol. II, p. 1627-1630

[8] J. Bajaj, L.O. Bubulac, P.R. Newman, W.E. Tennant, J. Vc. Sci. Technol. A 5(5), Sept/Oct 1987, 3186-3189

[9] W. Warta et al., Proc. 2nd WCEPSEC, Wien, 1650 (1998)